CrossMark

Analogue of Fano resonance and electromagnetically induced transparency in a graphene strip-ring compact resonator

Buzheng Wei[1,2] (ID) · Shuisheng Jian[1,2]

Abstract

A compact graphene strip-ring hybrid resonator working in the mid-infrared regime is proposed as an analogue of Fano resonator or electromagnetically induced transparency. The dipolar surface plasmon resonance induced by the ring interferes with the *x*-polarized strip resonance forming a symmetric or asymmetric transparency window within the absorption profile. The spectral response can be modulated not only by the Fermi energy level of graphene, but also the geometry shape of the configuration. The sensitivity reaches 2450 nm/RIU and the light in the transparency window is slowed down to over 1/1090 times the speed in vacuum. The analytic analysis is in accordance with the 3D simulation results. Our compact design may have potential view in optical sensors, optical switches and light storage field.

1 Introduction

Fano resonance or electromagnetically induced transparency (EIT) stands for a process when an autoionized discrete state interferes with a continuum one characteristically giving asymmetric or symmetric rise within the low absorption profile [1]. The findings of Fano or EIT resonance concentrate on the atomic use in early days, which hinders the application to a great extend due to its extreme experimental conditions and the difficulty to find proper nonlinear materials [2]. Recently, scientists and researchers focus on the classical manipulation of Fano- or EIT-like line shaped resonance intensively in plasmonic nanostructures [3] or metamaterials [4] and earn remarkable achievements both theoretically [5] and experimentally [6]. Most previous studies exhibit the analogy of quantum state interference in metastructures consisting of a bright mode and a dark mode [7]. The destructive interference happens in the bright mode because of the

different pathway transitions, which cancels the initial resonance. Meanwhile, the dark mode becomes populated [8] resulting in an asymmetric or symmetric transparency peak in the broad absorption spectral range. To achieve the direct interference between these two states, the mode resonators need to be well designed so that energy exchange happens in a specific way, mostly by breaking the structure symmetry. Alternatively, if the resonance in two mode resonators is factitiously led to interfere with one another [9], similar results can be observed but not following the analogue method mentioned above. It is more likely to be treated as the superposition of different resonances.

In our former researches [10–14], we have utilized graphene as a highly tunable material to excite graphene surface plasmon polaritons (SPPs) in metastructures and achieved EIT in several samples. As a famous candidate for newly emerged family of integrated metamaterials, graphene occupies an outstanding performance status embodying in its surface gate controlled conductivity [15], low dissipation loss [16], tighter interface localization [17] and ultra fast carrier mobilities at room temperature [18], only to name a few. Moreover, graphene possesses a 2-D electronic system composed of a single atomic layer of carbon atoms arranged in a hexagonal crystal lattice, which enables a gapless semiconducting property and a massless linear electron–hole dispersion [19]. Most inspiringly, different from electric or magnetic independent material that needs heating or pressure to change refractive index, permittivity or permeability, graphene's conductivity largely depends on passive

✉ Buzheng Wei
   14111010@bjtu.edu.cn

   Shuisheng Jian
   ssjian@bjtu.edu.cn

[1] Key Laboratory of All Optical Network and Advanced Telecommunication Network of EMC, School of Electronic Information and Engineering, Beijing Jiaotong University, Beijing 100044, China

[2] Institute of Lightwave Technology, Beijing Jiaotong University, Beijing 100044, China

chemical doping [20], active external static bias voltage or external static magnetic field [21]. This property ensures a wide tunable band from mid-infrared to terahertz regime without breaking or refabricating the device. Here, we list a few contributions related to graphene-based Fano resonance in recent years. Chae investigated the absorption of free-standing monolayer and bilayer graphene in ultraviolet region and the line shape was dominated by an asymmetric Fano resonance [22]. The excitonic resonance was attributed to couple to the Dirac continuum and the experimental data was quantitatively traced all way down to the infrared. Naresh fabricated a graphene-nanoantenna hybrid device which enabled efficient electrical modulation of Fano resonance at approximately 2 μ m and was numerically verified by full-wave 3D finite-element simulations [23]. Zheng proposed a new configuration of graphene-MoS$_2$ hybrid structure for ultrasensitive detection of molecules which displayed an enhancement factor of sensitivity by intensity more than 2 $\times 10^3$-fold when compared to the surface plasmon resonance sensing scheme [24]. These researches pave ways in many application areas such as sensing [25], optical storage [26], switching [27] and invisible cloaks [28].

In this letter, we report on a hybrid graphene strip-ring Fano or EIT resonator working in the mid-infrared regime, which consists of a graphene ring and a graphene strip located in its center. The formation mechanism is analytically and numerically investigated and the spectral responses

of which coincide with each other. Furthermore, this hybrid device is highly tunable with respect to the Fermi energy of graphene and is sensitive to outer refractive index. The geometric shape and the light source polarization direction also play important roles in modulating the resonances and they are investigated through numerical calculations as well. Finally ,we investigate the slow light effect within the transparency window and obtain a high group index. Conclusions are drawn at the end.

2 Formation mechanism

The proposed structure is schematically illustrated in Fig. 1. A graphene strip resonator is surrounded by a graphene ring resonator in the center periodically in x- and y-direction and they are buried in a dispersionless material. As one can see from the unit cell that the strip and ring can be both x-polarized excited when the surface plasmon are induced. However, the damping frequency difference and the oscillation wavelength between them are huge, which significantly shapes the Lorentzian lines if they are separately stimulated as indicated by the color lines in Fig. 1d. Since the outer ring has higher damping and higher loss, the spectral response is wider and shallower compared to the strip. Therefore, the ring resonant mode can be treated as the continuum state and the strip mode is treated as the discrete state. Nevertheless,

Fig. 1 **a** Zoomed in x–y view of a unit cell. The strip lies in the center of the ring with length L = 200 nm and width H = 50 nm. The outer radius of the ring is R = 250 nm and the width of which is w = 100 nm. The unit period in x and y direction is $P_x = P_y = 600$ nm throughout this paper. The electric field polarization angle with respect to x-direction is θ = 0. **b** The cut line x–z view from the brown dashed line in **a**. x-polarized electric field light source impinges from the top and propagates towards negative z direction. **c** The periodic structure in x–y plane. **d** The transmission when the Fermi energies of ring and strip are 0.8 and 0.3 eV, respectively. Green line: only ring is enabled. Brown line: only strip is enabled. Blue line: both resonators are enabled. Purple circle: analytic fitting according to Eq. (1)
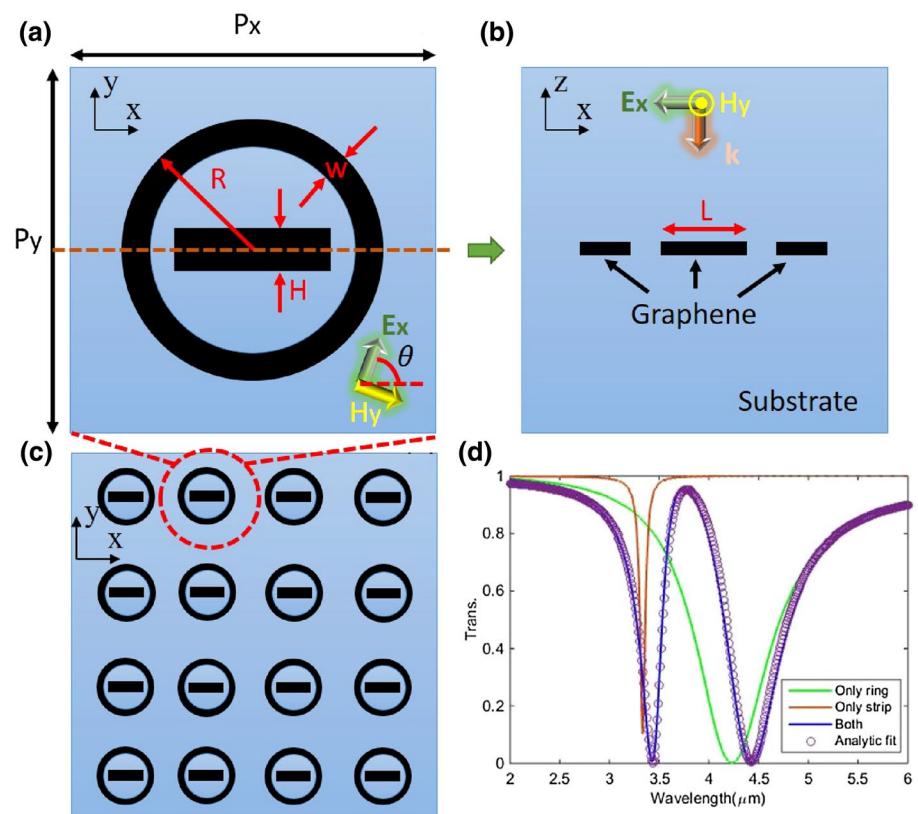
when both the resonators are excited at the same time, the mutually coupled surface wave changes the resonant condition by only either resonators and a rather pronounced Fano line is formed in the simulated region. An important parameter of the Fano system is the dephasing time calculated by $T_d = 2\hbar/\text{FWHM}$ [29, 30]. FWHM corresponds to the frequency domain full width half maximum and $\hbar$ is the reduced Planck's constant. For the transparency window in Fig. 1d, the dephasing time is 0.16 ps. To mathematically reveal the underlying physics, we use an analytic Fano interference model to quantify the simulated results. The transmission function T is given as $T = 1 - |t|^2$, where t is expressed as [31]

$$t = A + \sum_{i=1}^{\infty} \frac{a_i \Gamma_i e^{j\varphi_i}}{\omega - \omega_i + j\Gamma_i}, \tag{1}$$

here, A is the modulation amplitude, ω is the incident angular frequency and a_i, Γ_i, φ_i, ω_i are the amplitude, radiative damping, phase and angular resonant frequency of the ith oscillator representing the interfering hybridized resonances. In our structure, there only exists two resonators ($i = 1, 2$), the graphene ring and strip. So we fit the function into the blue line numerical results in Fig. 2d and obtain the fitting parameters as $A = 0.0985$, $a_1 = 0.93$, $\Gamma_1 = 30$ THz, $\varphi_1 = 1.5$, $\omega_1 = 4.299e14$ rad/s, $a_2 = 0.9$, $\Gamma_2 = 20$ THz, $\varphi_2 = 1.0$, $\omega_2 = 5.440e14$ rad/s. The fitting curve of the simulated Fano line in Fig. 2d are expressed by the circles. The geometry shape of the configuration and the substrate index (n_s) in this part are listed as: $n_s = 1.0$, $R = 250$ nm, $w = 100$ nm, $H = 50$ nm,

$L = 200$ nm and $\theta = 0$. The dielectric permittivity model of graphene is obtained by the data provided in FDTD that contains variables as graphene thickness, Fermi energy level and carrier mobility. The thickness of graphene is 0.335 nm according to the first exfoliation by Novoselov and Geim [32]. The Fermi energy of graphene ring (E_{fr}) is 0.8 eV while for the strip (E_{fs}) is 0.3 eV and the carrier mobility (μ) is rather conservative as 1 m^2/V/s [18, 33]. $P_x = P_y = 600$ nm is unchanged throughout this passage while other dielectric parameters and material properties of graphene in the simulation will be further discussed in the next section. In addition, the boundary is periodic in x- and y-direction while perfectly matched layers are built in z-direction in our Lumerical FDTD software.

To have a better view of the underlying physics, a more perceived electric and magnetic normalized field distribution plot is shown in Fig. 2. Since the electric field is x-polarized and the magnetic field is y-polarized, the surface dipolar resonances are in x- and y-direction, respectively. At transparency peak 3.746 µm, the outer ring resonance is strongly suppressed. The inner strip now acts as the dark mode that cancels the resonance in the bright ring resonator due the destructive interference. Otherwise, at two dips 3.424 and 4.425µm, both resonators exhibit strong oscillations. Though the surface resonances in both resonators are directly induced, it still presents apparent suppression between interference pathways. The light first couples to the ring and then exchanges with the strip. When the light couples back from the strip, the antiphase wave destructively interferes with the wave in the ring giving sharp rise in the
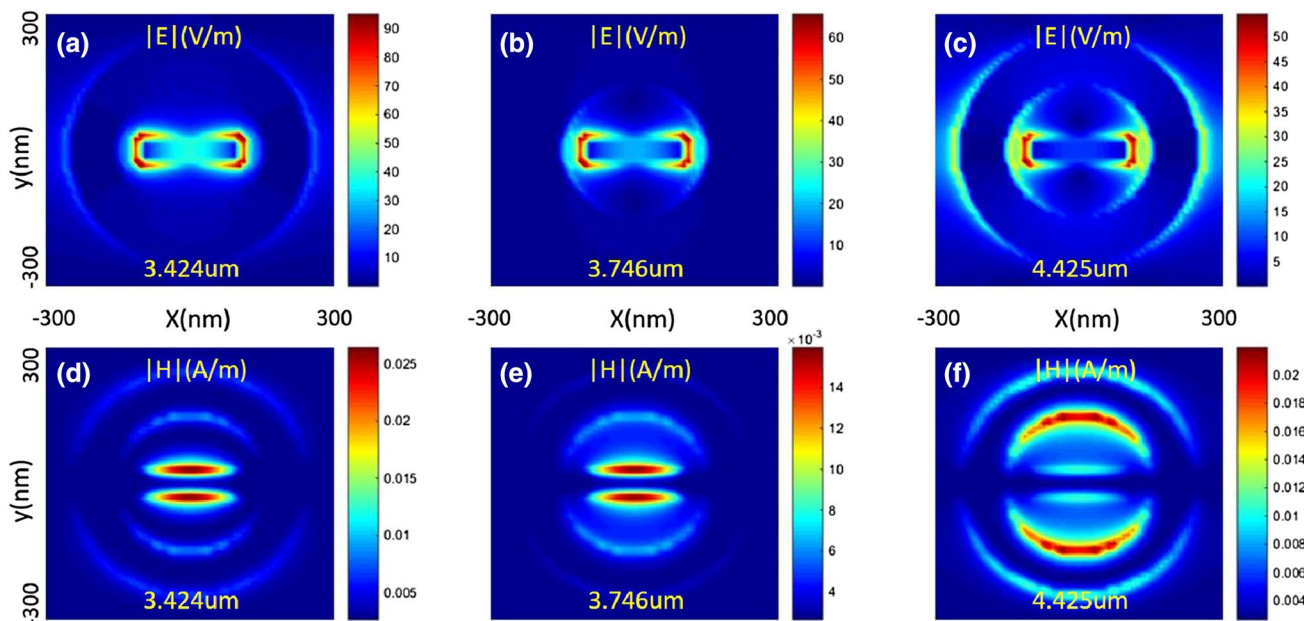

Fig. 2 The electric (**a**–**c**) and magnetic (**d**–**f**) field distributions at specific points on the blue line in Fig. 1d

absorption window. Hence, the structure here remains a classical analogy of Fano or EIT to some extent.

3 Simulations and applications

To precisely get a better control of the proposed device, several simulation tests on the material properties and the geometrical shape parameters require to be carefully examined. The 3D simulation here uses the finite difference time domain method (FDTD). First of all, as mentioned in the above section, the Fermi energy level and the carrier mobility have a relationship with the scattering rate which influences the surface conductivity of graphene significantly. To our acknowledgement, the carrier mobility using the chemical vapor deposition (CVD) method is always below $1 \, m^2/V/s$, while in the exfoliated graphene, it can exceed $23 \, m^2/V/s$ [18]. Since the simulation band lies in the mid-infrared regime, the interband transitions can be neglected according the famous Kubo formula [34]. Hence, the lower

carrier mobility is, the higher intrinsic loss is generated resulting in a relatively low transparency level and a higher resonant dip [35]. To numerically verify this deduction, we vary only the carrier mobility and keep other parameters unchanged as in Fig. 1. The Fano line shape variation is presented in Fig. 3a. One can notice that the carrier mobility here influences the strip resonant depth stronger than the ring's. Other than a lower transmission level, a small red shift of the transparency window center wavelength is accompanied. Next, because the Fermi energy level has the same impact on the resonant wavelength shift tendency of both ring and strip, for convenience, we only discuss the strip Fermi energy variation influence as an example. In Fig. 3b, the narrower stop band induced by the strip blue shifts with the increase of Fermi energy obviously and for 0.2 eV, the strip induced resonance lies in the longer wavelength region to the graphene ring resonance. The line shape of this condition is more symmetric compared to others. The farther separation of the eigen oscillation wavelengths of either resonators, the narrower strip resonance is observed.
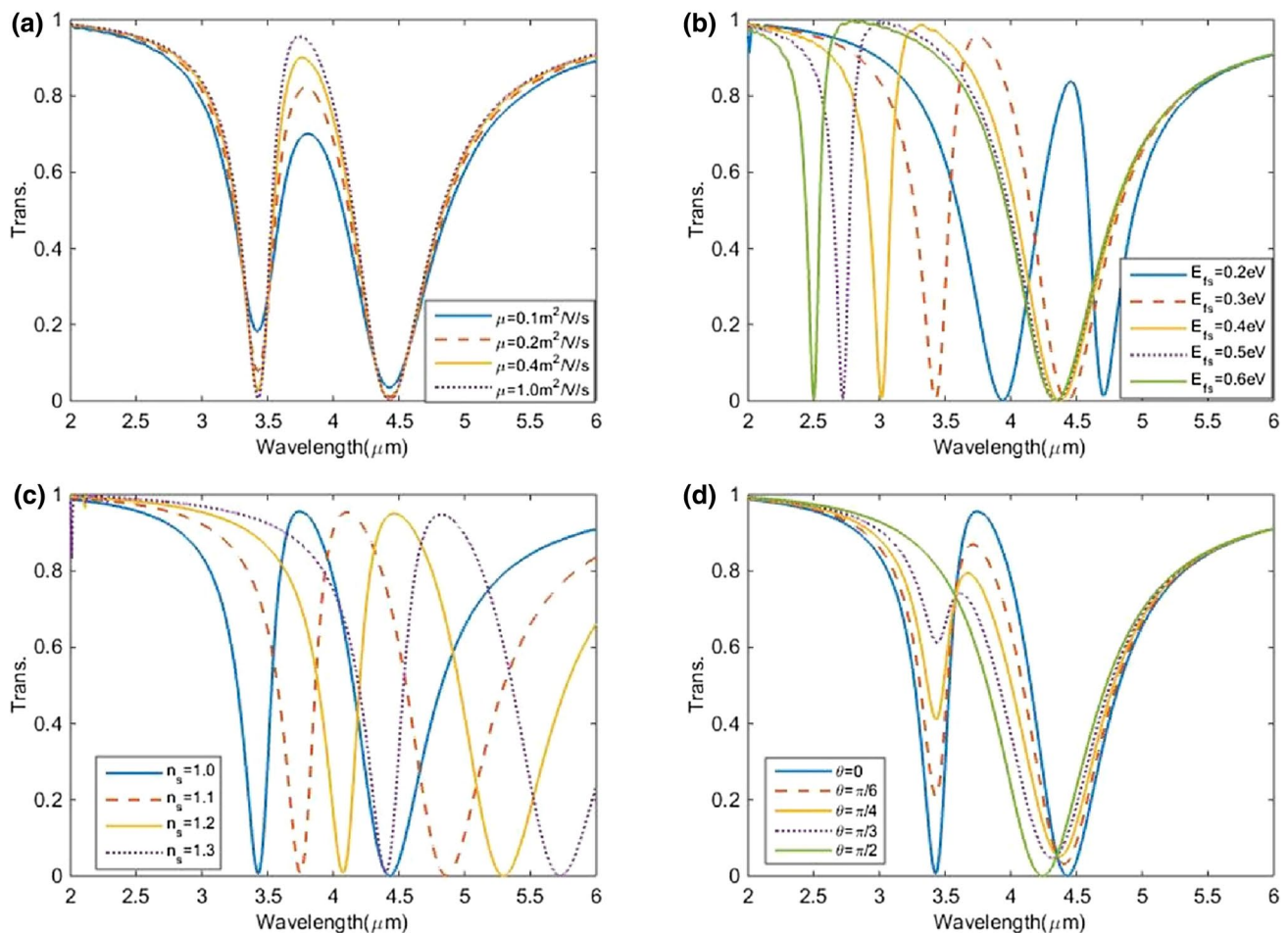

Fig. 3 Transmission spectra under different **a** carrier mobilities, **b** Fermi energy of the strip, **c** substrate index and **d** electric field polarization direction. When one parameter changes, others keep unchanged as those in Fig. 1

However, the Fermi energy change does not influence the resonant depth but brings a higher transparency level when it increases.

Second, as a potential application, the device can be applied to detect the refractive index change of the substrate. As depicted in Fig. 3c, when the substrate index increases from 1.0 to 1.3, the whole transmissions spectrum red shifts towards longer wavelength region without breaking the line shape. Other parameters are the same as in Fig. 1. One can calculate the sensitivity with respect to the refractive index change per unit (RIU) as $S = \Delta\lambda/\Delta\mathrm{RI}$, where $\Delta\lambda$ and $\Delta\mathrm{RI}$ are the resonant wavelength and index change accordingly. From the simulation data we can obtain that for this device, S equals 2450 nm/RIU. As a certain cognition, most of the biomolecules have their vibrational modes oscillating at THz frequencies [36], the device we design has a considerable compact size and works from mid infrared to THz regime which paves the way for its biosensing applications.

For all the above discussions, the electric field is polarized in x-direction and the strip surface plasmon is directly induced. Now, we vary the electric field polarization direction from x-direction to y-direction parallel in x–y plane, i.e., from TE mode to TM mode, with the step of 30° and check the transmission responses. As indicated by Fig. 3d, when the incident electric field polarization angle increases, the strip resonance becomes weaker successively. When the electric field is totally y-direction polarized, the strip induced surface plasmon is not excited and the spectral response only remains the resonance induced by the outer graphene ring. One can take advantage of the light source polarization direction to realize the switching function of the narrower stop band induced by the strip and to control the intensity of the transmitted light.

Except for the above discussions about the material properties and polarization angle, the geometry of the configuration also plays an important role in modulating the line shape of the spectrum. Obviously, there are four influential structural parameters: the ring radius, the ring width, the strip length and the strip height. The transmission spectra when one of these four parameters changes at a time are plotted in Fig. 4. Substantially, the change of geometry influences the eigen resonant wavelength, trip phase shift and the damping frequency of either resonators. Taking the ring for example, when the radius decreases, the resonant wavelength blue shifts with a narrower stop band. For $R = 230$ nm, a rather symmetric EIT line shape is observed. Because the distance between the two resonators draws closer, the interference intensity gets stronger. The shorter trip length results in a smaller phase shift and a lower damping. Together, a

narrower ring induced resonance is, therefore, modulated. This principle can be equivalently applied to other three sets of parameters and in each set of variation, there exists at least one symmetric EIT shape transmission line. From this point of view, the transition from Fano to EIT depends closely on the geometry adjustment which significantly modulates the eigen oscillation properties of either resonators. The superposition of the strip and ring induced resonance finally forms the desired line shape of transmission spectrum.

As a most inspiring companion, the light within the transparency window is always highly dispersive and ultra slow. By taking the phase shift numerical results Φ into calculation [10], the group index $n_g = c\tau/L_t$ is obtained and depicted in Fig. 5b. c stands for vacuum light speed, $\tau = \mathrm{d}\Phi/\mathrm{d}\omega$ is the group delay and L_t is the total trip length from source to monitor. The geometry parameters follow those in Fig. 1. A two π phase shift, which is caused by the interference of the mutually coupled resonators, happens at three crucial points of Fig. 2, respectively, and within the transparency window, the group index is beyond 1098 which means that the light is efficiently slowed down to 1/1098 times the speed in vacuum. However, at stop bands, a negative group index indicates that the light is speed up adjacent to the transparency window. Therefore, if the light traps at transparency window meets the modulation of Fermi energy, the change may shift transparency to transmission dips, so the stored light is released faster than the vacuum light to the output port. In this way, a flexible storage and release of light is objectively designed and the operation speed remains to be challenged in real experiments.

4 Conclusion

In this letter, a graphene strip-ring hybridized resonator is proposed to mimic Fano- or EIT-like resonance in the mid-infrared regime. The destructive interference between the dipolar ring resonance and strip polarized resonance gives rise in the absorption window. The device can be dynamically tuned by changing the Fermi energy level of graphene and the sensitivity is 2450 nm/RIU. The electric field polarization direction and the geometry shape modulate the line shape of transmittance and a slow light effect is observed within the transparency window of over 1/1098 times the speed in vacuum. The analytic results coincide well with the numerical ones carried out in the FDTD simulation software. These findings may pave way for optical sensing, switching and light storage field.
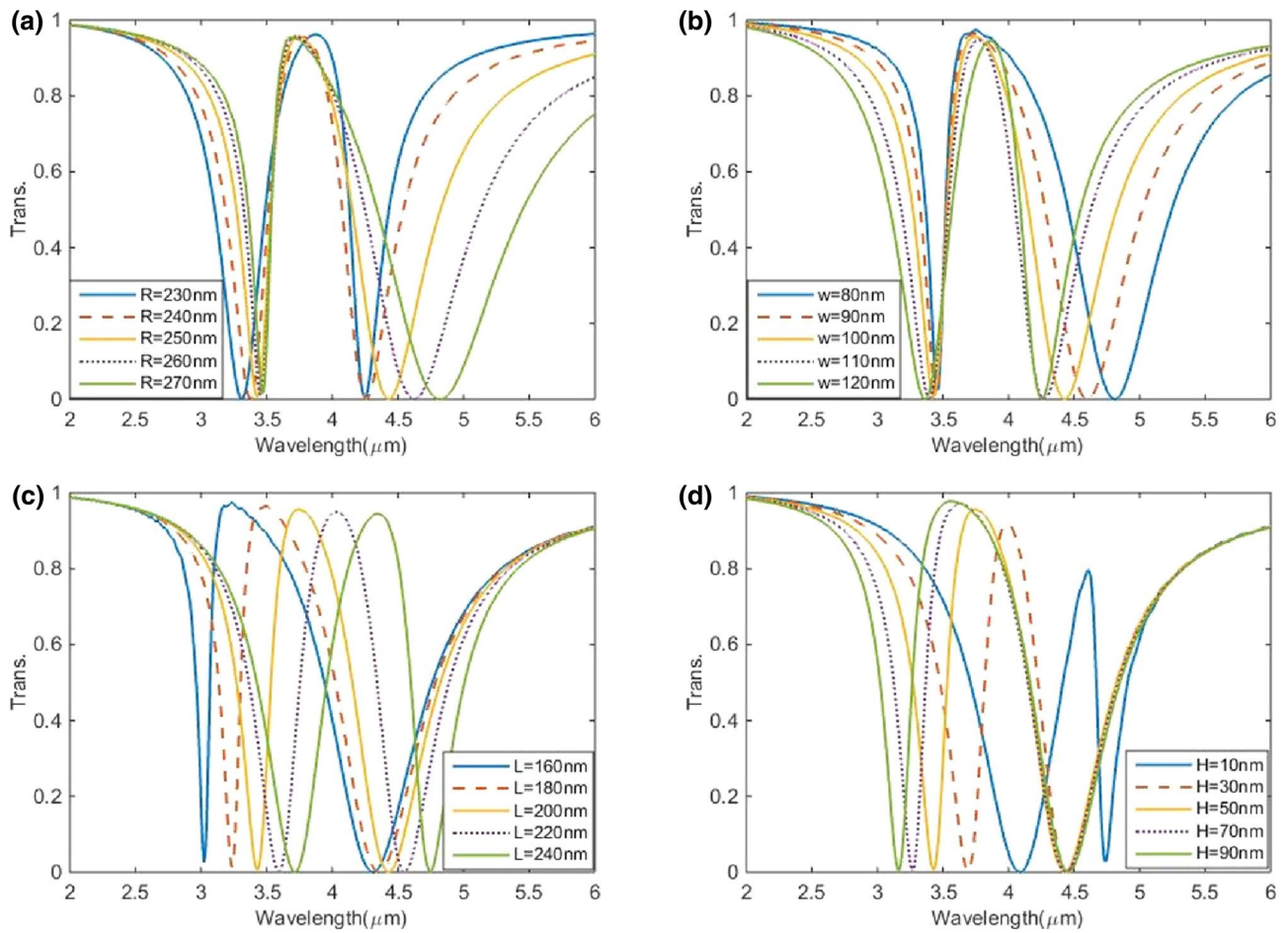
(a)

(b)

(c)

(d)

Fig. 4 Transmission spectra under different **a** ring radius *R*, **b** ring width *w*, **c** strip length *L* and **d** strip height *H*. When one parameter changes, others keep unchanged as those in Fig. 1
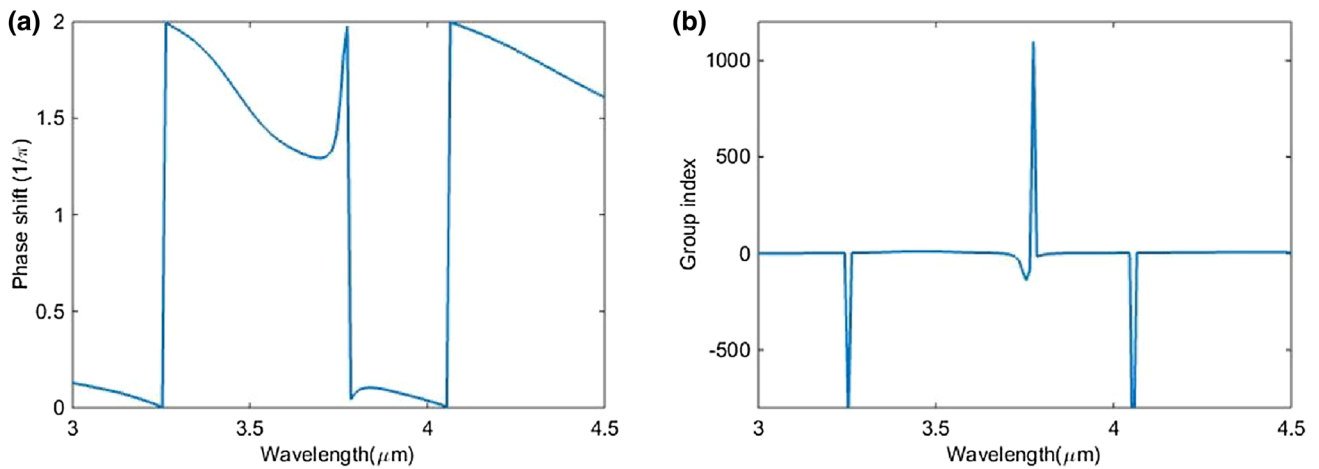
(a)

(b)

Fig. 5 **a** The phase shift and **b** the group index of Fig. 1

References

1. U. Fano, Phys. Rev. **124**, 1866 (1961)
2. N. Papasimakis, N.I. Zheludev, Opt. Photon. News **20**, 22 (2009)
3. B. Luk'yanchuk, N.I. Zheludev, S.A. Maier, N.J. Halas, P. Nordlander, H. Giessen, C.T. Chong, Nat. Mater. **9**, 707–715 (2010)
4. A.E. Miroshnichenko, S. Flach, Y.S. Kivshar, Rev. Mod. Phys. **82**, 2257 (2010)
5. S. Fan, W. Suh, J.D. Joannopoulos, J. Opt. Soc. Am. A: **20**, 569 (2003)
6. B. Peng, S.K. Özdemir, W. Chen, F. Nori, L. Yang, Nat. Commun. **5**, 5082 (2014)
7. M. Rahmani, B. Luk'yanchuk, M. Hong, Laser Photon. Rev. **7**, 329 (2013)
8. K.J. Boller, A. Imamoğlu, S.E. Harris, Phys. Rev. Lett. **66**, 2593 (1991)
9. Z. Zhang, G.I. Ng, T. Hu, H. Qiu, X. Guo, W. Wang, M.S. Rouifed, C. Liu, H. Wang, Appl. Phys. Lett. **111**, 081105 (2017)
10. B. Wei, S. Jian, J. Opt. **19**, 115001 (2017)
11. B. Wei, S. Jian, J. Phys. D Appl. Phys. **50**, 355101 (2017)
12. B. Wei, H. Liu, G. Ren, Y. Yang, S. Ye, L. Pei, S. Jian, Phys. Lett. A **381**, 160 (2017)
13. B. Wei, S. Jian, J. Nanophoton. **11**, 026011 (2017)
14. B. Wei, S. Jian, Opt. Commun. **402**, 66 (2017)
15. J. Horng, C.F. Chen, B. Geng, C. Girit, Y. Zhang, Z. Hao, H.A. Bechtel, M. Martin, A. Zettl, M.F. Crommie, Y.R. Shen, F. Wang, Phys. Rev. B **83**, 165113 (2011)
16. A. Vakil, N. Engheta, Science **332**, 1291 (2011)
17. M. Jablan, H. Buljan, M. Soljačiéc, Phys. Rev. B **80**, 245435 (2009)
18. K.I. Bolotin, K.J. Sikes, Z. Jiang, M. Klima, G. Fudenberg, J. Hone, P. Kim, H.L. Stormer, Solid State Commun. **146**, 351 (2008)
19. P.Y. Chen, A. Al, ACS Nano **5**, 5855 (2011)
20. L.A. Falkovsky, S.S. Pershoguba, Phys. Rev. B **76**, 153410 (2007)
21. G.W. Hanson, I.E.E.E. Trans, Antennas Propag. **56**, 747 (2008)
22. D.H. Chae, T. Utikal, S. Weisenburger, H. Giessen, K.V. Klitzing, M. Lippitz, J. Smet, Nano Lett. **11**, 1379–1382 (2011)
23. N.K. Emani, T.F. Chung, A.V. Kildishev, V.M. Shalaev, Y.P. Chen, A. Boltasseva, Nano Lett. **14**, 78–82 (2014)
24. G. Zheng, X. Zou, Y. Chen, L. Xu, W. Rao, Opt. Mater. **66**, 171 (2017)
25. Y. Zhang, T. Li, B. Zeng, H. Zhang, H. Lv, X. Huang, W. Zhang, A.K. Azad, Nanoscale **7**, 12682 (2015)
26. B. Wei, Y. Yang, S. Yao, H. Xiao, S. Jian, Appl. Phys. B **123**, 70 (2017)
27. M. Amin, M. Farhat, H. Baĝci, Sci. Rep. **3**, 2105 (2013)
28. S.J. Buzheng Wei, Opt. Eng. **56**, 56 (2017)
29. A. Ahmadivand, R. Sinha, B. Gerislioglu, M. Karabiyik, N. Pala, M. Shur, Opt. Lett. **41**(22), 5333 (2016)
30. F. Miyamaru, M. Tanaka, M. Hangyo, Phys. Rev. B **74**, 153416 (2006)
31. Y. Binfeng, H. Guohua, C. Jiawei, C. Yiping, Plasmonics **9**, 691 (2014)
32. A. Geim, K. Novoselov, Nat. Mater. **6**, 183–191 (2007)
33. K. Novoselov, V. Fal'ko, L. Colombo, P. Gellert, M. Schwab, K. Kim, Nature **490**, 192–200 (2012)
34. G.W. Hanson, J. Appl. Phys. **103**, 064302 (2008)
35. L.A. Falkovsky, A.A. Varlamov, Eur. Phys. J. B **56**, 281 (2007)
36. C. Wu, A.B. Khanikaev, R. Adato, N. Arju, A.A. Yanik, H. Altug, G. Shvets, Nat. Mater. **11**, 69–75 (2012)